RSC Advances

PAPER

View Article Online
View Journal | View Issue

Cite this: *RSC Adv.*, 2024, **14**, 2697

Engineering a hierarchically micro-/nanostructured Si@Au-based artificial enzyme with improved accessibility of active sites for enhanced catalysis†

Jian Wang,[a] Bo Ye,[b] Shiqi Xiao[b] and Xia Liu *[a]

Received 31st October 2023
Accepted 29th November 2023

DOI: 10.1039/d3ra07421h

rsc.li/rsc-advances

The active site accessibility and high loading of gold nanoparticles (AuNPs) are key factors affecting the catalytic activity of supported AuNP-based catalysts. However, the preparation of supported AuNP-based catalysts with highly accessible active sites still remains a challenge. Herein, sphere-on-sphere (SoS) silica microspheres with a hierarchical structure, good dispersion and high surface density of thiol groups (10 SH nm^{-2}) are prepared and used as a platform for the growth of high-density AuNPs. The obtained hierarchical Si@Au micro-/nanostructure consisting of 0.55 μm SoS silica microspheres and 7.3 nm AuNPs (SoS-0.55@Au-7.3) is found to show excellent peroxidase-mimicking activity (K_m = 0.033 mM and V_{max} = 34.6 × 10^{-8} M s^{-1}) with merits of high stability and good reusability. Furthermore, the as-obtained SoS-0.55@Au-7.3-based system can sensitively detect hydrogen peroxide (H_2O_2) with a low detection limit of 1.6 μM and a wide linear range from 2.5 μM to 1.0 mM. The high catalytic activity, excellent stability and good reusability of SoS-0.55@Au-7.3 imply its great prospects in biosensing and biomedical analysis.

1. Introduction

Enzymes, with good substrate specificity and efficient catalytic activities, have attracted great interest in biosensing, pharmaceutical processes and food industry application. However, their practical applications are largely restricted owing to their sensitivity to changes in environmental conditions and relatively low stability. Under the impetus of these factors, artificial enzymes are developed to mimic the complex properties of natural enzymes. Due to their stability and cost-effectiveness, artificial enzymes have become ideal substitutes for natural enzymes and have promising applications in the fields of biosensing, bionics and biomedicine.[1–4]

During recent decades, various catalytic nanomaterials, such as gold nanoparticles (AuNPs),[5,6] cerium oxide nanoparticles,[7,8] magnetic nanoparticles,[9,10] platinum nanomaterials,[11,12] and metal–organic frameworks[13,14] have been discovered as candidates for high-efficiency artificial enzymes. Among these, AuNPs have attracted tremendous research interest due to their exceptional biocompatibility, controlled catalytic activity, and the accessibility of various biofunctionalization.[15–17] However, the catalytic activity of AuNPs is susceptible since they easily aggregate when directly introduced into the reaction system because of their large specific surface area.[1] In addition, the practical application of AuNPs catalysts is seriously limited by the difficulty to separate and recover them from the reaction solution.[18] It is a promising strategy to improve the dispersibility and reusability of bare AuNPs by anchoring AuNPs on supporting materials.[19] Currently, the commonly used carriers for anchoring AuNPs mainly include carbon,[20] silica,[21] and polymers.[22] Among them, silica is an ideal carrier for anchoring AuNPs since its rich silanols (Si–OH) can be facilely functionalized by other chemical groups (*e.g.* –SH, $–NH_2$).[23,24] Currently, mesoporous silica has been developed to load high-content AuNPs for improving their catalytic activity.[25] However, there is a risk of blockage and poor accessibility of Au active sites because mesoporous silica pores have a typical tubular structure, which seriously affects their catalytic activity.[26] Recently, catalysts with a hierarchical structure have attracted intense attention due to their improved accessibility of active sites.[27–29] For instance, Jiang and co-workers synthesized anatase TiO_2 hierarchical nanostructured microspheres by a two-step process of electrospray and hydrothermal method.[30] The hierarchical structure not only increases the local concentration of active sites on the material surface, but also facilitates the diffusion of liquid-phase reactants and products, which effectively improves the photocatalytic activity.[31–33] Inspired by this, constructing supported AuNPs-based catalysts with

[a]*School of Chemistry, Southwest Jiaotong University, Chengdu 610031, China. E-mail: xliu@swjtu.edu.cn*

[b]*College of Life Science and Engineering, Southwest Jiaotong University, Chengdu 610031, China*

† Electronic supplementary information (ESI) available: Details on the preparation of materials, characterization, optimization of experimental conditions, statistical analysis and additional figures. See DOI: https://doi.org/10.1039/d3ra07421h

a hierarchical structure and high loading might be an efficient way to enhance the catalytic activity.

In this study, SoS silica microspheres with submicron-scale are prepared by a simple one-pot method using (3-mercaptopropyl) trimethoxysilane (MPTMS) as the silica precursor. The SoS silica microspheres have a hierarchical structure, good dispersion and high surface density of thiol groups (10 SH nm^{-2}), exhibiting a high loading capacity of AuNPs. The as-obtained SoS-0.55@Au-7.3 composed of 0.55 μm SoS silica microspheres and 7.3 nm AuNPs shows excellent peroxidase-mimicking activity, high stability and good reusability. Furthermore, a SoS-0.55@Au-7.3-based colorimetric method can be used for quantitatively detecting H_2O_2 and exhibit a wide concentration range from 2.5 μM to 1.0 mM with a very low detection limit (1.6 μM). The results demonstrate that the hierarchical Si@Au micro-/nanostructures shed light on the potential effective utilization strategy of AuNPs in biosensing and biomedical analysis.

2. Experimental section

2.1. Materials

All chemicals were used in the same manner as received and were not further processed. Poly(vinyl alcohol) (PVA, 80% DA, 9–10 kDa), (3-mercaptopropyl) trimethoxysilane (MPTMS, 95%), ammonium hydroxide solution (28–30% NH_3 basis), and cetyltrimethylammonium bromide (CTAB ≥ 98%) were purchased from Sigma-Aldrich. Sodium acetate, tetraethyl orthosilicate (TEOS), sodium borohydride ($NaBH_4$), Au(III) chloride hydrate ($HAuCl_4$), 5,5′-dithiobis (2-nitrobenzoic acid) ($DTNB^{2-}$) and 3,3′,5,5′-tetramethylbenzidine (TMB) were purchased from Adamas. Hydrogen peroxide (30%), methanol and ethanol (analytical purity) were purchased from Chengdu Dingsheng Times Company. Deionized (DI) water (>18.2 MΩ cm) was used for all experiments.

2.2. Preparation of SoS silica microspheres

SoS silica microspheres were produced using the previously described approach with minor changes.[34] Briefly, 0.25 g of PVA is rapidly dissolved in water (5 mL) by sonication. CTAB (0.2 g) was added to the solution with magnetic stirring. After CTAB was fully dissolved, methanol (8 mL) and ammonium hydroxide (2 mL, 5.6%) were added to the solution in order. After the mixed solution was stirred for 15 min, a certain amount of MPTMS was dropped in slowly within 15 s. The reaction was kept being stirred at ambient temperature for 24 h. After centrifugation at 5000 rpm for 3 min and three washes using ethanol and deionized water, the pure solid products were collected. The obtained pure solid product was then put into a vacuum drying oven for 12 h at 37 °C to finally obtain SoS silica microspheres. In order to obtain dispersed SoS silica microspheres, a series of SoS silica microspheres with different sizes were synthesized by varying the reaction dose of MPTMS with the other synthesis parameters unchanged, which were named SoS-*X*, and *X* is the size of the SoS silica microsphere (Table S1†).

To investigate the contribution of the structure and surface thiol density of the silica microspheres to the loading of AuNPs, smooth silica microspheres with low surface thiol density (SSM-L) were synthesized using a post-grafting method[35,36] and smooth silica microspheres with high surface thiol density (SSM-H) were also synthesized using the one-pot synthesis without CTAB (see details in ESI†).[34]

2.3. Immobilization of AuNPs on SoS silica microspheres

AuNPs-loaded SoS silica microspheres according to the previous method reported in the literature.[15] The synthesized SoS-0.55 silica microspheres (20 mg) were ultrasonically dispersed in a certain amount of water (as shown in Table S3†) for 10 min. After the solution was stirred for 15 min, 0.5 mL $HAuCl_4$ solution (0.1 M) was added and stirred continuously for 1 h. Subsequently, cold $NaBH_4$ solution prepared freshly was quickly added. After reaction for 1 h, the resulting solution was centrifuged at 5000 rpm and washed three times using ethanol and deionized water to remove the reaction residues. After vacuum drying at 37 °C for 6 h, the obtained SoS-0.55@Au was stored in an inert atmosphere. In order to optimize the loading of AuNPs on the surface of SoS-0.55 silica microspheres, a series of AuNPs loaded SoS-0.55 silica microspheres was synthesized by adding various amount of $HAuCl_4$ and $NaBH_4$ (as shown in Table S3†) while other synthetic parameters remain unchanged. The obtained product is named as SoS-0.55@Au-s, with s representing the size of AuNPs loaded on the surface of SoS-0.55 silica microspheres.

3. Results and discussion

3.1. Preparation and characterization of SoS silica microspheres

SoS silica microspheres were produced by a one-pot method reported by the previous literature, during which PVA, CTAB, NH_3 H_2O, and MPTMS were respectively used as stabilizer, structure guide, catalyst, and silica precursor (Scheme S1†).[34] The SEM image in Fig. 1a shows that the as-obtained SoS silica microspheres are uniform in size (0.55 μm, named SoS-0.55 silica microspheres). The SoS silica microspheres have hierarchical structures, which are composed of large spheres and small spheres wrapped in an outer layer of large spheres. As shown in Fig. 1b, the TEM image of SoS silica microspheres shows good dispersion and rough surface structure. The phenomenon further proves the hierarchical structures of the SoS silica microspheres. The TEM elemental mappings and energy dispersive X-ray spectroscopy (EDS) indicate uniform distribution of Si, O, and S elements (Fig. 1c–f and S1†). As shown in Fig. 1g, the FTIR spectrum of SoS silica microspheres show the absorption bands at 3425 cm^{-1} and 1630 cm^{-1} (vibrational band of Si–OH), 1128 cm^{-1} (stretching mode of the Si–O bond), 806 cm^{-1} and 470 cm^{-1} (vibrational mode of SiO_2).[34] The stretching vibration bands of C–H (2930 cm^{-1}) and S–H (2557 cm^{-1}) and the bands in the 1260–1200 cm^{-1} region are characteristic vibrations of silicon–alkyl bonds, indicating that the SoS silica microspheres are organic–inorganic hybrid

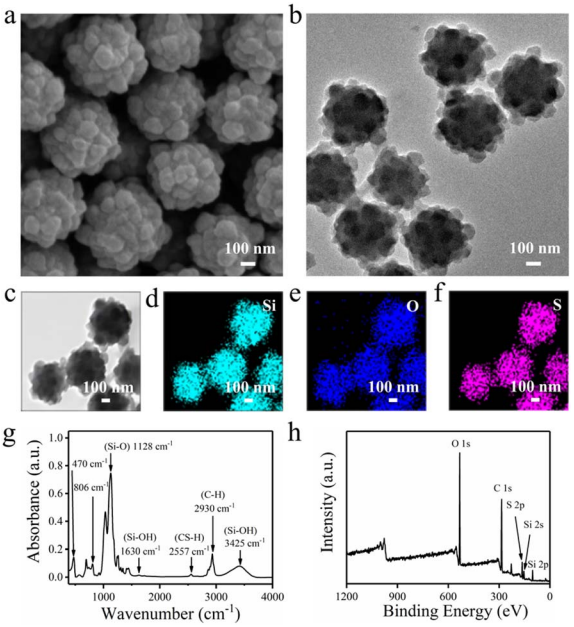

Fig. 1 (a) SEM and (b) TEM images of SoS-0.55 silica microspheres. (c) DF STEM image and (d–f) TEM elemental mappings of SoS-0.55 silica microspheres. (g) FTIR spectrum and (h) XPS spectra of SoS-0.55 silica microspheres.

silica materials formed by PVA and MPTMS.[34,37] These results demonstrate that SoS silica microspheres with hierarchical structures can be successfully obtained using a one-pot synthesis from MPTMS.

To study how the concentration of MPTMS influences the size and morphology of silica microspheres, different concentrations of MPTMS were used to prepare silica microspheres (Table S1†). The SEM images (as shown in Fig. S2†) show that the as-obtained microspheres in each synthesis are uniform in size (0.50, 0.55, 1.20, 2.30, and 5.50 μm, respectively). The results indicate that the size of microspheres is increased by increasing the concentration of MPTMS. When the concentration of MPTMS is greater than 12.6 mM, the large spheres are densely coated by the small spheres, which means that SoS-*X* (*X* = 0.55, 1.20, 2.30, and 5.50 μm) silica microspheres have hierarchical structures. To obtain dispersed SoS silica microspheres, the stability of SoS-*X* (*X* = 0.55, 1.20, 2.30, and 5.50 μm) silica microspheres in aqueous solution was studied.[38] A remarkable decrease of the relative absorbance is observed for the microspheres (*X* > 1 μm), while the microspheres (*X* < 1 μm) have no obvious change (Fig. S3†). The results indicate that the SoS-0.55 silica microsphere not only has a hierarchical structure, but also can maintain good dispersion in its aqueous suspensions, which is important in mimicking enzyme-catalyzed reactions in aqueous environments. Thus, the SoS-0.55 silica microspheres will be used for further study.

The XPS spectra of SoS-0.55 silica microspheres in Fig. 1h show the XPS peaks of O 1s (~530 eV), C 1s (~284 eV), S 2p (~163 eV), Si 2s (~153 eV) and Si 2p (~101 eV).[25] The sulfur content on the outer surface of SoS-0.55 silica microspheres by XPS analysis is 6.05 wt%. In order to determine the number of free thiol groups on the surface of microspheres, the spectroscopic method invented by Ellman was applied.[39] As shown in Fig. S4,† the conversion of 5,5′-dithiobis (2-nitrobenzoic acid) ($DTNB^{2-}$) to (2-nitro-5-thiobenzoic acid) dianion (NTB^{2-}) can be detected by UV-Vis spectroscopy due to the presence of thiols on the surface of SoS-0.55 silica microspheres, and the absorbance of NTB^{2-} at 412 nm directly correlates with the amount of free thiols.[40,41] The Ellman test results show that the thiol group density on the outer surface of SoS-0.55 silica microspheres is 151.6 μmol g^{-1}. N_2 adsorption–desorption isotherms of SoS-0.55 silica microspheres showed type V isotherms (Fig. S5†). Combined with the BET specific surface area test result (9.6 m^2 g^{-1}) (Fig. S5†), it is calculated that the average surface density of thiol groups is 10 SH nm^{-2}, which is higher than the previously reported values.[25,42–44] The results exhibit that the SoS-0.55 silica microspheres have a high surface density of thiol groups, which is very favorable for the loading process of AuNPs.[45,46]

3.2. Synthesis and characterization of AuNPs-loaded SoS-0.55 microspheres

SoS-0.55 silica microspheres have an open hierarchical structure and a high surface thiol group density, which makes them ideal carriers for *in situ* loading of AuNPs. The hierarchical structure of SoS-0.55 silica microspheres facilitates the easy access of gold chloride ions to the carrier surface, and the high surface thiol group density (10 SH nm^{-2}) is more favorable for the formation of S–Au covalent bonds between thiol groups and gold chloride ions, which are then reduced *in situ* by $NaBH_4$, resulting in the formation of high-density AuNPs. As shown in Fig. 2a and b, the TEM images show that the surface morphology of SoS-0.55 silica microspheres does not change significantly after loading AuNPs. The high-resolution TEM image (Fig. 2c) shows that AuNPs with a diameter of 7.3 nm (determined by the measured size of 100 AuNPs as shown in Fig. S6†) are densely distributed on the microsphere surface without fusing into larger particles. Fig. 2d shows the crystal structure of AuNPs. The measured lattice spacing value of 0.23 nm are ascribed to Au(111) planes.[47] These results demonstrate the successful acquisition of AuNPs-loaded SoS-0.55 silica microspheres (SoS-0.55@Au-7.3) with hierarchical micro-/nanostructures. As shown in Fig. 2e–h, the DF-STEM image and TEM elemental mappings of SoS-0.55@Au-7.3 show the uniform distribution of Si, S, and Au elements. The EDS also confirms that the SoS-0.55@Au-7.3 is made up of Si, O, S, C, and Au elements (Fig. S7†).

The UV-Vis spectroscopy, XPS and XRD were used to further validate the structure of SoS-0.55@Au-7.3. As shown in Fig. S8,† SoS-0.55@Au-7.3 has an UV-Vis absorption peak at 550 nm, which is the characteristic plasma resonance band of silica microsphere-supported AuNPs, indicating that SoS-0.55 silica microspheres are loaded with AuNPs.[48] As shown in Fig. 2i, the XRD spectrum has four strong diffraction peaks (2θ = 38°, 45°, 65° and 78°), corresponding to the Bragg diffraction of the crystal plane of AuNPs (110), (200), (220), and (311), respectively, which also confirms the existence of AuNPs.[15] XPS spectral peaks in Fig. 2j are Au 4f (83 eV), S 2p (163 eV), C 1s (284 eV), O

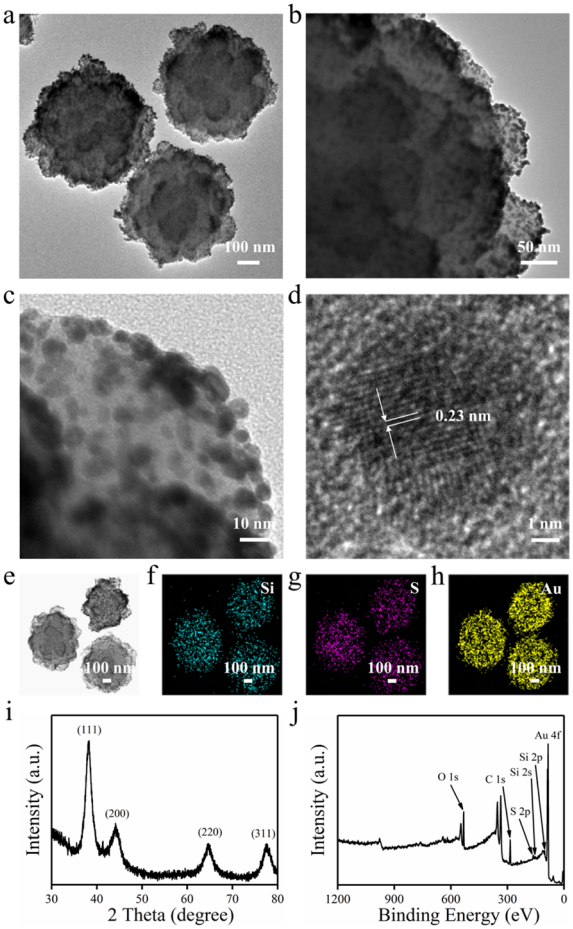

Fig. 2 (a–d) TEM images of the SoS-0.55@Au-7.3 under different magnifications. (e) DF STEM image and (f–h) TEM elemental mappings of SoS-0.55@Au-7.3. (i) XRD pattern, and (j) XPS spectra of SoS-0.55@Au-7.3.

1s (530 eV), Si 2s (153 eV) and Si 2p (101 eV), respectively.[25] The presence of the Au 4f peaks also clearly indicates the successful loading of AuNPs on SoS-0.55 silica microspheres. The Au content on the outer surface of SoS-0.55@Au-7.3 by XPS measurement is 14.50 wt%, which is comparable with the previously reported values.[49] The result indicates the advantage of the high surface thiol density and the hierarchical structure of SoS-0.55 silica microspheres for supporting AuNPs.

To evaluate the contribution of the surface thiol density and hierarchical structure to the Au loading capacity of silica microspheres, smooth silica microspheres with low surface thiol density (SSM-L, 31.1 μmol g^{-1}) and smooth silica microspheres with high surface thiol density (SSM-H, 144.9 μmol g^{-1}) were prepared for comparison (see Fig. S4 and Experimental section in ESI†). After loading AuNPs, the Au content of SSM-L@Au-7.8 is measured to be 2.61 wt%, which is much lower than that for SSM-H@Au-7.6 (11.28 wt%) (Fig. S9 and Table S2†), suggesting that the content of loaded AuNPs is directly connected with the density of thiol groups. Note that the surface thiol density of SSM-H is approximately the same as that of SoS-0.55 (151.6 μmol g^{-1}). However, the Au content of SSM-H@Au-7.6 (11.28 wt%) is lower than that of SoS-0.55@Au-7.3 (14.50 wt%) (Table S2†). It is expected that the hierarchical structure of the SoS-0.55 silica microsphere may raise the local concentration of thiol groups in reaction solution and enhance reaction efficiency of thiol groups and gold chloride ions.[50] Therefore, the high thiol density and hierarchical structure of SoS-0.55 silica microspheres are two important factors to improve the loading content of AuNPs.

3.3. Peroxidase activity of SoS-0.55@Au

To evaluate the peroxidase-like activity of SoS-0.55@Au, the catalytic oxidation reaction of the 3,3′,5,5′-tetramethylbenzidine (TMB) substrate was carried out.[15] As shown in Fig. 3a and b, SoS-0.55@Au-7.3 catalyzes TMB oxidation in the presence of H_2O_2 and the color of the solution changes from colorless to blue, with the maximum absorbance at 652 nm, proving that SoS-0.55@Au-7.3 has a peroxidase-like activity. Under the same conditions, the SoS-0.55 silica microspheres is unable to catalyze the conversion of TMB to the oxidized TMB (oxTMB), indicating that the inherent catalytic activity of SoS-0.55@Au-7.3 comes from AuNPs. Furthermore, by comparing the peroxidase activities of SSM-L@Au-7.8, SSM-H@Au-7.6 and SoS-0.55@Au-7.3 under the same conditions (Fig. 3b), it can be found that SoS-0.55@Au-7.3 has the highest peroxidase activity. These results suggest that the high Au loading and hierarchical micro-/nanostructures of SoS-0.55@Au-7.3 is beneficial for enhancing the peroxidase-like activity.

To further investigate the contribution of the Au loading of SoS-0.55 silica microspheres on their enzymatic catalytic

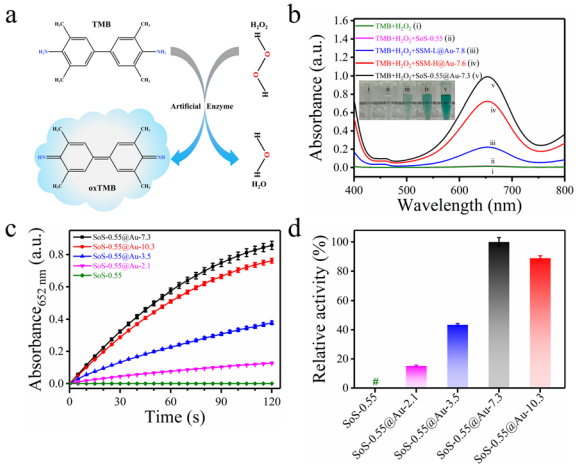

Fig. 3 (a) Schematic illustration of the oxidization of colorless TMB to blue-colored oxTMB catalyzed by artificial enzyme in the presence of H_2O_2. (b) The absorbance spectra and apparent color changes of the oxTMB in various reaction systems: (i) TMB + H_2O_2, (ii) TMB + H_2O_2 + SoS-0.55, (iii) TMB + H_2O_2 + SSM-L@Au-7.8, (iv) TMB + H_2O_2 + SSM-H@Au-7.6 and (v) TMB + H_2O_2 + SoS-0.55@Au-7.3 in 0.1 M sodium acetate buffer (pH 4) at 35 °C. (c) The absorbance of the oxTMB at 652 nm as the function of time for the SoS-0.55 silica microsphere and SoS-0.55@Au-*s* and (d) the relative activities corresponding to the SoS-0.55 silica microsphere and SoS-0.55@Au-*s*. The absorbance for SoS-0.55@Au-*s* to that for SoS-0.55@-7.3 was used to define the relative activity.

activity, different concentrations of $HAuCl_4$ were used to synthesis SoS-0.55 silica microspheres with different Au content. By varying the initial amount of $HAuCl_4$, a series of SoS-0.55@Au-*s* ($s = 2.1 \pm 0.1$, 3.5 ± 0.1, 7.3 ± 0.2 and 10.3 ± 0.1 nm) were synthesized (Fig. S6 and Table S3†). Their Au loadings are 1.97, 8.06, 14.50, and 20.47 wt%, respectively, as measured by XPS (Table S2†). The results indicate that the Au loading of SoS-0.55 silica microspheres increases with the increase of $HAuCl_4$ concentration, indicating that SoS-0.55 silica microspheres have a high loading capacity of AuNPs. The peroxidase-like activity of SoS-0.55@Au-*s* was investigated by measuring the increase of the absorbance at 652 nm using UV-Vis spectroscopy after the reaction of the same amount of TMB and H_2O_2. Fig. 3c displays the absorbance of the oxTMB at 652 nm as a function of time at the same mass concentration of SoS-0.55@Au-*s*. The increase in the absorbance of the oxTMB over time indicates that SoS-0.55@Au-*s* has an inherent peroxidase-like activity. As shown in Fig. 3d, the relative activities of SoS-0.55, SoS-0.55@Au-2.1, 3.5, 7.3 and 10.3 are 0, 0.15, 0.43, 1.00 and 0.89, respectively, showing that the peroxidase-like activity of SoS-0.55@Au-*s* gradually increases with the increase of the Au loading from 1.97% to 14.50%, and the peroxidase-like activity of SoS-0.55@Au-7.3 reaches the maximum when the Au loading is 14.50%. The enzymatic activity of SoS-0.55@Au-10.3 is significantly weakened though the highest gold loading is reached. This is mainly because the surface-active sites of large-sized Au nanoparticles are significantly reduced.[25] These results demonstrate that SoS-0.55@Au-7.3 loading a high content of small AuNPs shows the highest activity.

To further investigate the high peroxidase-like activity of SoS-0.55@Au-7.3, the initial rate method was used to study the steady-state kinetics and determine the kinetic parameters.

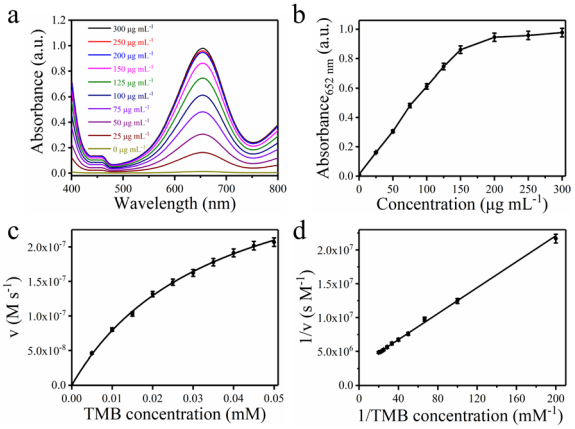

Fig. 4 (a) The absorption spectra corresponding to the oxTMB generated by different concentrations of the SoS-0.55@Au-7.3. (b) The absorbance of the oxTMB at 652 nm as a function of the concentration of SoS-0.55@Au-7.3. (c) Steady-state kinetic assay of SoS-0.55@Au-7.3. Experiments were performed in 0.1 M sodium acetate buffer (pH 4) with 200 μg mL^{-1} SoS-0.55@Au-7.3, 50 mM H_2O_2 and varied concentrations of TMB at 35 °C. (d) Lineweaver–Burk plot of the inverse of the initial rate *vs.* the inverse of the substrate concentration for estimating the kinetic parameters (K_m and V_{max}) of SoS-0.55@Au-7.3 using TMB as the substrate.

Fig. 4a and b shows the absorption spectra of the oxTMB generated by different concentrations of SoS-0.55@Au-7.3. The result indicates that the catalytic activity of SoS-0.55@Au-7.3 increases with increasing its concentration from 0 to 200 μg mL^{-1} (Fig. S10†). The increase of catalytic activity is not evident when the concentration is greater than 200 μg mL^{-1}, which may be due to the poor dispersion of particles with the excessive concentration.[26] The Michaelis–Menten kinetics were verified and monitored by varying the concentration of TMB at a SoS-0.55@Au-7.3 concentration of 200 μg mL^{-1}. Fig. 4c, d and S11† show the Michaelis–Menten steady-state dynamics plot and the Lineweaver–Burk plot, respectively. For the peroxidase-acting substrate TMB, SoS-0.55@Au-7.3 achieves a K_m of 0.033 mM and a V_{max} of 34.6×10^{-8} M s^{-1}. Compared with the native enzyme (HRP, 0.041 mM), the K_m value of SoS-0.55@Au-7.3 is significantly reduced, indicating that it has better substrate affinity for TMB.[51] This is mainly due to the fact that SoS-0.55@Au-7.3 has a high Au loading and hierarchical micro-/nanostructure, which not only increases the local active site, but also facilitates the special diffusion of substrates and products, thereby promoting the catalytic performance.[26] Furthermore, the V_{max} value of SoS-0.55@Au-7.3 (~8 times that of HRP, 4.3×10^{-8} M s^{-1}) is significantly higher than those of the recently reported artificial enzymes (Table S4†).[15,25,26,51–55] This indicates that SoS-0.55@Au-7.3 has a high enzymatic catalytic activity with the help of the hierarchical micro-/nanostructures and the high loading of AuNPs.

3.4. Stability of SoS-0.55@Au-7.3

The stability of SoS-0.55@Au-7.3 is of great significance for its practical application.[56] To study the effect of pH and temperature on the enzymatic activity, SoS-0.55@Au-7.3 was preconditioned in buffers with different pH values and temperatures before testing the catalytic activity. As shown in Fig. 5a, SoS-0.55@Au-7.3 exhibits the highest peroxidase-like activity at pH 3. In neutral solution (pH 7), SoS-0.55@Au-7.3 maintains about

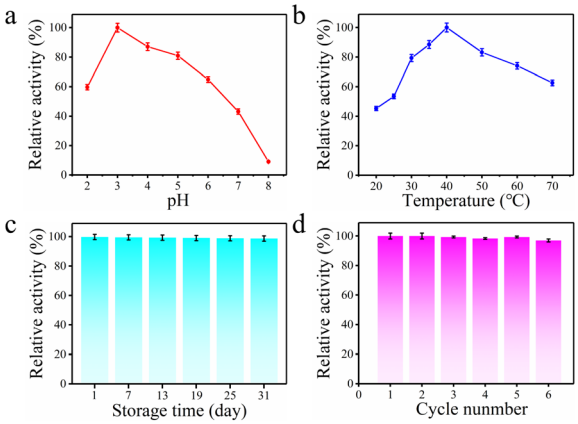

Fig. 5 The effect of pH (a) and temperature (b) on the peroxidase-like activity of SoS-0.55@Au-7.3. (c) The peroxidase-like activity of SoS-0.55@Au-7.3 after being left for different number of days (d) reusability assay of SoS-0.55@Au-7.3 in sodium acetate buffer (pH 4). The error bars represent standard deviation ($n = 3$).

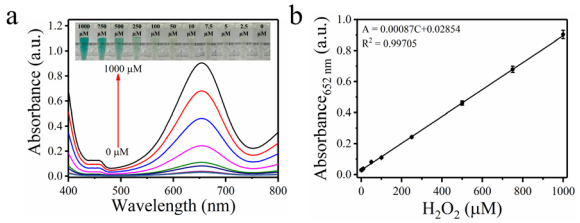

Fig. 6 (a) UV-visible spectra and color variations of the TMB oxidation system in the existence of SoS-0.55@Au-7.3 in the concentration scope of H_2O_2 from 0 to 1000 μM in sodium acetate buffer at pH 3. (b) The linear diagram for H_2O_2 detection.

42% of the peroxidase-like activity at pH 3. Furthermore, SoS-0.55@Au-7.3 shows the highest peroxidase-like activity at 40 °C, and maintains 94% of the highest peroxidase-like activity at physiological temperature of 37 °C (Fig. 5b). The results suggest that SoS-0.55@Au-7.3 has a good enzyme activity over a wide pH and temperature range. To further verify the storage stability, the catalytic activity of SoS-0.55@Au-7.3 was tested after 31 days storage. Fig. 5c shows that SoS-0.55@Au-7.3 retains 98% of its original activity, indicating the long-time storage stability of SoS-0.55@Au-7.3. Besides, SoS-0.55@Au-7.3 have a relatively large size (about 0.55 μm in diameter), so it is easy to separate them from the reacting mixtures by centrifugation for reuse. And the remanent catalytic activity of SoS-0.55@Au-7.3 keep 97% of initial activity after the 6th reacting cycles (Fig. 5d), demonstrating that SoS-0.55@Au-7.3 has a good reusability. These results demonstrate that SoS-0.55@Au-7.3 is an efficient, stable and recyclable artificial enzyme, which is superior to natural enzymes.

3.5. Detection of hydrogen peroxide

Hydrogen peroxide (H_2O_2), as one of the important reactive oxygen species, is present in many biological processes. It tends to accumulate within the mitochondria, which is intimately related to many diseases, such as Parkinson's, Alzheimer's diseases and cancer.[57] In this study, based on the high peroxidase activity and stability of SoS-0.55@Au-7.3, a spectrophotometric detection of H_2O_2 was carried out. As shown in Fig. 6a, the absorbance of the oxTMB at 652 nm gradually increases with increasing H_2O_2 concentration, suggesting that the catalytic activity of SoS-0.55@Au-7.3 is H_2O_2 concentration-dependent. Fig. 6b exhibits a wide linear relationship between the H_2O_2 concentration (from 2.5 to 1000 μM) and the absorbance (correlation coefficient $R^2 = 0.99705$), and the detection limit of H_2O_2 is 1.6 μM ($3\sigma/s$), which is lower than or comparative with previously reported values (Table S5†).[58–62] These results imply that the SoS-0.55@Au-7.3 shows a highly sensitive response towards the concentration change of H_2O_2.

4. Conclusions

In conclusion, SoS silica microspheres with the high surface density of accessible thiol groups are successfully prepared by a facile one-pot synthesis method in the presence of MPTMS and CTAB. The SoS-0.55 silica microspheres are capable of loading high-density AuNPs with small size and have good dispersibility. The obtained SoS-0.55@Au-7.3 has a hierarchical micro-/nanostructure, which not only increases the local active site, but also provides enhanced accessibility of the substrate. The experimental results demonstrate that SoS-0.55@Au-7.3 exhibits the highest peroxidase-like activity. Furthermore, SoS-0.55@Au-7.3 has good stability and can remain the relatively high activity after multiple cycles of use. This study offers a feasible approach to achieve the low-cost application of AuNP-based high-efficiency artificial enzymes in biosensors, analytical devices, and industrial catalysis.

Author contributions

J. Wang and X. Liu conceived and designed the project. J. Wang performed the sample fabrication, characterization and data analysis. B. Ye and S. Q. Xiao provided assistance in the sample fabrication and characterization. All authors contributed to the analysis and discussion of the experimental results. J. Wang wrote the manuscript, and all authors revised the final version.

Conflicts of interest

The authors declare no conflict of interest.

Acknowledgements

This work was supported by the National Natural Science Foundation of China (21903065), the Sichuan Science and Technology Program (2021YFH0125) and the Fundamental Research Funds for the Central Universities (2682022ZTPY033). The authors would like to thank Analysis and Testing Center of Southwest Jiaotong University for the SEM test.

Notes and references

1 Y. Lin, J. Ren and X. Qu, *Adv. Mater.*, 2014, **26**, 4200–4217.
2 F. Cao, L. Jin, Y. Gao, Y. Ding, H. Wen, Z. Qian, C. Zhang, L. Hong, H. Yang, J. Zhang, Z. Tong, W. Wang, X. Chen and Z. Mao, *Nat. Nanotechnol.*, 2023, **18**, 617–627.
3 Y. Zeng, H. Yue, B. Cao, Y. Li, M. Yang and C. Mao, *Angew. Chem., Int. Ed.*, 2022, **61**, e202210121.
4 L. Zhang, H. Wang and X. Qu, *Adv. Mater.*, 2023, 2211147.
5 H. Sheng, J. Wang, J. Huang, Z. Li, G. Ren, L. Zhang, L. Yu, M. Zhao, X. Li, G. Li, N. Wang, C. Shen and G. Lu, *Nat. Commun.*, 2023, **14**, 1528–1539.
6 J. P. Horwath, C. Lehman Chong, A. Vojvodic and E. A. Stach, *ACS Nano*, 2023, **17**, 8098–8107.
7 C. Yao, Y. Xu, J. Tang, P. Hu, H. Qi and D. Yang, *Nat. Commun.*, 2022, **13**, 7739–7751.
8 Z. Luo, Y. Zhou, T. Yang, Y. Gao, P. Kumar and R. Chandrawati, *Small*, 2022, **18**, 2105762–2105771.
9 K. S. Park, M. I. Kim, D. Y. Cho and H. G. Park, *Small*, 2011, **7**, 1521–1525.
10 Z. Chen, J. J. Yin, Y. T. Zhou, Y. Zhang, L. Song, M. Song, S. Hu and N. Gu, *ACS Nano*, 2012, **6**, 4001–4012.

11 L. Zhang, L. Laug, W. Münchgesang, E. Pippel, U. Gösele, M. Brandsch and M. Knez, *Nano Lett.*, 2010, **10**, 219–223.
12 J. Fan, J. J. Yin, B. Ning, X. Wu, Y. Hu, M. Ferrari, G. J. Anderson, J. Wei, Y. Zhao and G. Nie, *Biomaterials*, 2011, **32**, 1611–1618.
13 J. Wu, Y. Yu, Y. Cheng, C. Cheng, Y. Zhang, B. Jiang, X. Zhao, L. Miao and H. Wei, *Angew. Chem., Int. Ed.*, 2021, **60**, 1659.
14 L. Qin, X. Wang, Y. Liu and H. Wei, *Anal. Chem.*, 2018, **90**, 9983–9989.
15 Y. Tao, E. Ju, J. Ren and X. Qu, *Adv. Mater.*, 2015, **27**, 1097–1104.
16 Y. Guo, J. Zhang, J. Liu, N. Wang and X. Su, *Anal. Chim. Acta*, 2023, **1276**, 341649–341657.
17 Z. Wu, C. Dong, Y. Li, H. Hao, H. Zhang, Z. Lu and B. Yang, *Angew. Chem., Int. Ed.*, 2013, **52**, 9952–9955.
18 Y. Ye, M. Jin and D. Wan, *J. Mater. Chem. A*, 2015, **3**, 13519–13525.
19 A. Corma and H. Garcia, *Chem. Soc. Rev.*, 2008, **37**, 2096–2126.
20 J. E. Perea Buceta, T. Wirtanen, O. V. Laukkanen, M. K. Mäkelä, M. Nieger, M. Melchionna, N. Huittinen, J. A. LopezSanchez and J. Helaja, *Angew. Chem., Int. Ed.*, 2013, **125**, 12051–12055.
21 Y. Zhang, J. Zhang, B. Zhang, R. Si, B. Han, F. Hong, Y. Niu, L. Sun, L. Li, B. Qiao, K. Sun, J. Huang and M. Haruta, *Nat. Commun.*, 2020, **11**, 558–567.
22 C. Yuan, W. Luo, L. Zhong, H. Deng, J. Liu, Y. Xu and L. Dai, *Angew. Chem., Int. Ed.*, 2011, **50**, 3515–3519.
23 P. Munnik, P. E. de Jongh and K. P. de Jong, *Chem. Rev.*, 2015, **115**, 6687–6718.
24 M. B. Gawande, A. Goswami, T. Asefa, H. Guo, A. V. Biradar, D. L. Peng, R. Zboril and R. S. Varma, *Chem. Soc. Rev.*, 2015, **44**, 7540–7590.
25 M. Kalantari, T. Ghosh, Y. Liu, J. Zhang, J. Zou, C. Lei and C. Yu, *ACS Appl. Mater. Interfaces*, 2019, **11**, 13264–13272.
26 R. Singh, R. Belgamwar, M. Dhiman and V. Polshettiwar, *J. Mater. Chem. B*, 2018, **6**, 1600–1604.
27 D. G. Montjoy, E. A. K. Wilson, H. Hou, J. D. Graves and N. A. Kotov, *Nat. Commun.*, 2023, **14**, 857–866.
28 N. Bayal, R. Singh and V. Polshettiwar, *ChemSusChem*, 2017, **10**, 2182–2191.
29 R. Singh, R. Bapat, L. Qin, H. Feng and V. Polshettiwar, *ACS Catal.*, 2016, **6**, 2770–2784.
30 Q. Jiang, J. Huang, B. Ma, Z. Yang, T. Zhang and X. Wang, *Colloids Surf., A*, 2020, **602**, 125112.
31 D. Shen, J. Yang, X. Li, L. Zhou, R. Zhang, W. Li, L. Chen, R. Wang, F. Zhang and D. Zhao, *Nano Lett.*, 2014, **14**, 923–932.
32 X. Du and S. Z. Qiao, *Small*, 2015, **11**, 392–413.
33 A. Maity and V. Polshettiwar, *ChemSusChem*, 2017, **10**, 3866–3913.
34 A. Ahmed, H. Ritchie, P. Myers and H. Zhang, *Adv. Mater.*, 2012, **24**, 6042–6048.
35 W. Stöber, A. Fink and E. Bohn, *J. Colloid Interface Sci.*, 1968, **26**, 62–69.
36 R. L. Oliveira, W. He, R. J. M. Klein Gebbink and K. P. de Jong, *Catal. Sci. Technol.*, 2015, **5**, 1919–1928.
37 G. I. Andrade, E. F. Barbosa Stancioli, A. A. P. Mansur, W. L. Vasconcelos and H. S. Mansur, *J. Mater. Sci.*, 2008, **43**, 450–463.
38 S. Jatav, K. P. Furlan, J. Liu and E. H. Hill, *ACS Appl. Mater. Interfaces*, 2020, **12**, 19813–19822.
39 X. D. Wang, K. S. Rabe, I. Ahmed and C. M. Niemeyer, *Adv. Mater.*, 2015, **27**, 7945–7950.
40 M. Moser, T. Behnke, C. Hamers Allin, K. Klein Hartwig, J. Falkenhagen and U. Resch Genger, *Anal. Chem.*, 2015, **87**, 9376–9383.
41 M. Moser, R. Schneider, T. Behnke, T. Schneider, J. Falkenhagen and U. Resch Genger, *Anal. Chem.*, 2016, **88**, 8624–8631.
42 P. Yang, Y. Shu, Q. Zhuang, Y. Li and J. Gu, *Chem. Commun.*, 2019, **55**, 12972–12975.
43 K. Fu, X. Liu, C. Lv, J. Luo, M. Sun, S. Luo and J. C. Crittenden, *Environ. Sci. Technol.*, 2022, **56**, 2677–2688.
44 R. Liang and H. Zou, *RSC Adv.*, 2020, **10**, 18534–18542.
45 M. S. Inkpen, Z. F. Liu, H. Li, L. M. Campos, J. B. Neaton and L. Venkataraman, *Nat. Chem.*, 2019, **11**, 351–358.
46 G. Pacchioni, *Nat. Rev. Mater.*, 2019, **4**, 226.
47 Z. Wang, Q. Zhang, D. Kuehner, A. Ivaska and L. Niu, *Green Chem.*, 2008, **10**, 907–909.
48 M. Dhiman, B. Chalke and V. Polshettiwar, *J. Mater. Chem. A*, 2017, **5**, 1935–1940.
49 Z. Chen, H. Ji, C. Liu, W. Bing, Z. Wang and X. Qu, *Angew. Chem., Int. Ed.*, 2016, **55**, 10732–10736.
50 A. Bard, R. Rondon, D. T. Marquez, A. E. Lanterna and J. C. Scaiano, *Photochem. Photobiol.*, 2018, **94**, 1109–1115.
51 M. Liu, H. Zhao, S. Chen, H. Yu and X. Quan, *ACS Nano*, 2012, **6**, 3142–3151.
52 L. Gao, J. Zhuang, L. Nie, J. Zhang, Y. Zhang, N. Gu, T. Wang, J. Feng, D. Yang, S. Perrett and X. Yan, *Nat. Nanotechnol.*, 2007, **2**, 577–583.
53 Y. Song, K. Qu, C. Zhao, J. Ren and X. Qu, *Adv. Mater.*, 2010, **22**, 2206–2210.
54 Y. M. Wang, J. W. Liu, J. H. Jiang and W. Zhong, *Anal. Bioanal. Chem.*, 2017, **409**, 4225–4232.
55 W. Shi, Q. Wang, Y. Long, Z. Cheng, S. Chen, H. Zheng and Y. Huang, *Chem. Commun.*, 2011, **47**, 6695–6697.
56 R. Chapman and M. H. Stenzel, *J. Am. Chem. Soc.*, 2019, **141**, 2754–2769.
57 Y. Wu, P. Balasubramanian, Z. Wang, J. A. S. Coelho, M. Prslja, R. Siebert, M. B. Plenio, F. Jelezko and T. Weil, *J. Am. Chem. Soc.*, 2022, **144**, 12642–12651.
58 Y. Wang, D. Zhang and J. Wang, *Microchim. Acta*, 2017, **185**, 1–8.
59 L. J. Peng, H. Y. Zhou, C. Y. Zhang and F. Q. Yang, *Colloids Surf., A*, 2022, **647**, 129031–129038.
60 H. Zhao, Y. Dong, P. Jiang, G. Wang and J. Zhang, *ACS Appl. Mater. Interfaces*, 2015, **7**, 6451–6461.
61 M. Nasir, S. Rauf, N. Muhammad, M. Hasnain Nawaz, A. Anwar Chaudhry, M. Hamza Malik, S. Ahmad Shahid and A. Hayat, *J. Colloid Interface Sci.*, 2017, **505**, 1147–1157.
62 T. Niu, X. Deng, R. Wang and C. Zhou, *Mater. Today Chem.*, 2018, **7**, 35–39.